Reprinted from JOURNAL OF APPLIED MECHANICS, *Vol. 47, No. 1, March 1980*

K. J. Bathe
Associate Professor.

C. A. Almeida
Graduate Student.

Department of Mechanical Engineering,
Massachusetts Institute of Technology,
Cambridge, Mass. 02139

A Simple and Effective Pipe Elbow Element—Linear Analysis

The formulation of a new, simple, and effective displacement-based pipe bend element is presented. The displacement assumptions are axial, torsional, and bending displacements that vary cubically along the axis of the elbow with plane sections remaining plane, and a generalization of the von Karman pipe radial displacement patterns to include the ovalization effects. The amount of ovalization varies cubically along the elbow with full compatibility between elbows. The pipe bend element has been implemented, and the results of various sample analyses are presented, which illustrate the effectiveness of the element.

1 Introduction

The structural integrity and cost of pipelines are of major concern in the nuclear, oil, and various other industries. Pipelines can be subjected to severe thermal, seismic, and other mechanical loads, and for these reasons, an increasing amount of attention has been given to their analyses [1].

In the analysis of pipelines it is convenient to distinguish between the straight and curved portions of the pipe. The straight portions of the pipeline can, in general, be adequately represented by simple beam elements with circular cross sections. However, the bend components of the pipe are much more difficult to analyze, because, in addition to undergoing the usual beam deformations, the pipe bends also ovalize. This ovalization affects the flexibility of a pipe bend a great amount and must be properly modeled in the analysis [2–8].

Because of the importance and the difficulties that lie in the analysis and design of pipe bends, much research has been devoted to the study of their structural behavior. In these investigations, during recent years, also various simple to complex finite-element models of pipe bends have been proposed. However, all these structural models have serious limitations either with regard to their accuracy in predicting pipe stresses and displacements or the cost of using them.

The simplest and widely used approach in the linear analysis of pipelines is to model a pipe bend using simple curved beam theory and scale the stiffness constants and calculated stresses using factors that account for the ovalization of the pipe cross section and the pipe internal pressure [5]. If the effect of the internal pressure can be neglected, the constants used in this analysis are, in essence, the von Karman flexibility and stress-intensification factors [6]. These constants were derived by von Karman for in-plane loading and later by Vigness using the von Karman analysis procedure for out-of-plane loading [2] with a number of assumptions. A major point is that von Karman considered a differential length of the elbow in which the internal bending moment is constant. Therefore, if the factors are applied to a complete elbow, it is assumed that the ovalization is constant along the pipe bend. The conditions of a varying magnitude in the internal bending moment and the fact that there may be no ovalization at the end of the elbow cannot be taken into account with accuracy.

Because of the limitations of the foregoing beam analysis of pipe bends various refined analytical and finite-element models have been proposed [5,7]. In essence, these models use shell theory to describe the behavior of the pipe bend. Clark and Reissner proposed equations that treat pipe bends as part of a torus and proposed an asymptotic solution for the stress and flexibility factors [8]. This approach removes some of the assumptions of the von Karman analysis but is not effective in the analysis of general pipelines. The greatest potential for the general analysis of pipe bends lies in the use of the finite-element method [9]. Pipe elbows are currently being modeled using three-dimensional elements, general shell elements, and special elbow-shell elements [10–13]. Using either three-dimensional or general shell elements, in theory, any elbow can be modeled very accurately by using a fine enough finite-element mesh. However, in practice, such an analysis of a simple elbow involves typically of the order of a thousand finite-element equilibrium equations that need be operated upon, which means that the linear analysis of a single elbow is very costly, the nonlinear analysis of a single elbow is prohibitively expensive and the nonlinear analysis of an assemblage of elbows is clearly beyond the current state-of-the-art of computational tools.

In order to reduce the number of finite-element variables special elbow-shell elements have been proposed [12]. Although these elements are more cost-effective in use, they still involve a relatively large

Contributed by the Applied Mechanics Division for publication in the JOURNAL OF APPLIED MECHANICS.

Discussion on this paper should be addressed to the Editorial Department, ASME, United Engineering Center, 345 East 47th Street, New York, N. Y. 10017, and will be accepted until June 1, 1980. Readers who need more time to prepare a discussion should request an extension from the Editorial Department. Manuscript received by ASME Applied Mechanics Division, April, 1979; final revision, July, 1979.

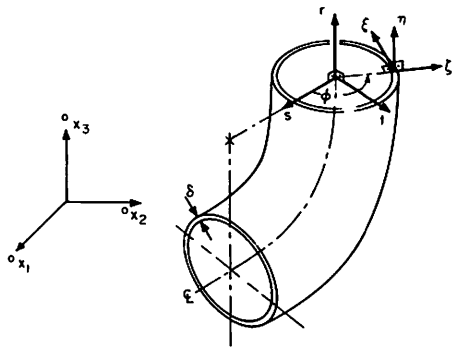

(a) COORDINATE SYSTEMS USED

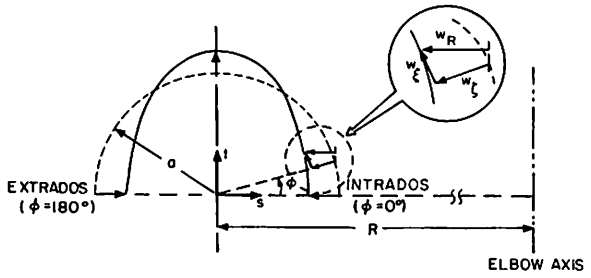

(b) DISPLACEMENTS OF DEFORMED CROSS SECTION (FIRST VON KARMAN MODE; w_ζ IS SHOWN NEGATIVE)

Fig. 1 Coordinate systems and displacements of elbow

number of solution variables and are subject to some major shortcomings, for example, the axial variation of the magnitude of ovalization is still neglected [12], or the rigid-body mode criterion is not satisfied [13].

The objective in this paper is to present the formulation of a new elbow element that is simple and effective and predicts accurately the significant deformations and stresses in various curved pipe segments. The elbow element is a four-node displacement-based finite element with axial, torsional, and bending displacements and the von Karman ovalization deformations all varying cubically along the elbow length. The formulation of the element is a very natural extension and generalization of von Karman's pioneering analysis [6]. In essence, von Karman analyzed in his work a differential length of pipe using the Ritz method to calculate the flexibility and stress-intensification factors. Because of the lack of the digital computer, von Karman could only consider in the Ritz analysis the hoop direction of the pipe, but it is interesting to note that von Karman "urges us engineers to become familiar with the Ritz method, because the method is simple and ideal to develop approximate solutions to complex practical problems" (quoted from reference [6]). The formulation of the new elbow element presented here extends the work of von Karman in that we use the Ritz method (the displacement-based finite-element method) to take also the axial variation of ovalization accurately into account, and relax some other von Karman assumptions. The actual analysis presented here is only possible because the digital computer is available and the analysis is performed efficiently using finite-element numerical procedures [9].

In this paper we consider only the linear analysis of piping systems. However, the full potential of the element lies in the geometric and material nonlinear analysis of pipes, because the element is very cost-effective and indeed allows an accurate nonlinear dynamic analysis of assemblages of pipe bends. The nonlinear formulation of the element, to be presented later, is based on the procedures given in [14, 15].

In the next section of this paper we briefly review the von Karman analysis with emphasis on the important concepts that we employ in the finite-element formulation of the new pipe elbow element. This formulation is presented in Section 3 of the paper. The elbow element has been implemented in the computer program ADINAP [16], and in Section 4 we present the analysis results of some problems that demonstrate the validity of the element.

2 The Theory of von Karman

The formulation of the pipe elbow element can be regarded as an extension of the von Karman analysis, the major concepts of which are for completeness briefly summarized in this section.

2.1 von Karman Assumptions. In his analysis of pipe elbows von Karman recognized that in addition to the usual curved beam theory strain components, two additional strain components also need be considered that are due to the ovalization of the cross section; see Fig. 1. These strain components are a pipe cross-sectional circumferential strain, $(\epsilon_{\xi\xi})_{ov}$, which is due to the deformation of the cross section, and a longitudinal strain, $(\epsilon_{\eta\eta})_{ov}$, which is due to the change in the curvature of the pipe itself. Corresponding to the usual strain components, the von Karman analysis is based on the following major assumptions.

1 Plane sections originally plane and normal to the neutral axis of the pipe are assumed to remain plane and normal to the neutral axis.

2 The longitudinal strains are assumed to be of constant magnitude through the pipe wall thickness.

3 The circumferential strains are assumed to vanish at the middle surface of the pipe wall, and are due to pure transverse bending of the pipe wall. Hence the pipe wall thickness is assumed to be small in comparison to the pipe external radius; i.e., $\delta/a \ll 1$.

4 The pipe external radius is assumed to be much smaller than the radius of the pipe bend; i.e., $a/R \ll 1$.

5 The effect of Poisson's ratio is neglected.

Using assumption 3, a relation can be written between the radial and circumferential displacements of the middle surface of the pipe wall,

$$w_\zeta = -\frac{dw_\xi}{d\phi} \tag{1}$$

where w_ζ is the radial displacement, w_ξ is the tangential displacement and ϕ measures the angular position considered as shown in Fig. 1.

2.2 von Karman Analysis. In his analysis von Karman established the strain energy in an element of pipe that is subjected to a constant bending moment, and used the Ritz method to estimate the amount of ovalization.

Using the assumptions previously summarized, the longitudinal strains due to the distortion of the cross section are

$$(\epsilon_{\eta\eta})_{ov} = \frac{w_R}{R} \tag{2}$$

where R is the pipe bend radius and w_R is the local displacement of the pipe wall in the bend radial direction, see Fig. 1. Also, the tangential strain component is

$$(\epsilon_{\xi\xi})_{ov} = -\frac{1}{a^2}\left[w_\zeta + \frac{d^2 w_\zeta}{d\phi^2}\right]\zeta \tag{3}$$

where a is the radius of the pipe and ζ is the local coordinate in the pipe wall, see Fig. 1.

Using equations (1)–(3) and assumptions 1–5, the total strain energy of an elbow of angle α is

$$V = \frac{Ea\delta R}{2}\int_0^\alpha \times\left\{\int_0^{2\pi}\underbrace{\left[-\left(\frac{\Delta\alpha}{R\alpha}\right)a\cos\phi\right]}_{\text{TERM 1}} + \underbrace{\frac{1}{R}\left(w_\xi\sin\phi + \frac{dw_\xi}{d\phi}\cos\phi\right)}_{\text{TERM 2}}\right]^2 d\phi, + \int_0^{2\pi}\underbrace{\left(\frac{\delta^2}{12}\right)\left[\frac{1}{a^2}\left(\frac{dw_\xi}{d\phi} + \frac{d^3 w_\xi}{d\phi^3}\right)\right]^2}_{\text{TERM 3}} d\phi\Bigg\} d\theta \tag{4}$$

Table 1 Number of ovalization shape functions to be used in Ritz analysis (and elbow formulation)

Geometric range	Number of functions N
$\lambda \geq 0.5$	1
$0.16 \leq \lambda < 0.5$	2
$0.08 \leq \lambda < 0.16$	3
$0.04 \leq \lambda < 0.08$	4

where δ is the pipe wall thickness, E is the Young's modulus of the material and $\Delta\alpha$ is the cross-sectional angular rotation. In equation (4) TERM 1 corresponds to the curved beam theory longitudinal strain, and TERM 2 and TERM 3 correspond to the straining that is due to ovalization.

The only variable in equation (4) is the displacement w_ξ. To estimate this displacement von Karman assumed for in-plane bending of the elbow

$$w_\xi = \sum_{n=1}^{N} c_i \sin 2n\phi \tag{5}$$

and performed a Ritz analysis to obtain the parameters c_i. The validity of the von Karman trial functions in equation (5) has been substantiated by experiments [2–4].

Considering the von Karman analysis, a geometric pipe factor λ, where $\lambda = R\delta/a^2$, plays an important role in the determination of the number of trial functions that should be included in the analysis. Table 1 summarizes the number of trial functions that need be used for different values of λ in order to obtain satisfactory results.

Considering the von Karman analysis, it may be noted that assumptions 2, 4, and 5 are not used in the formulation of the elbow element presented in the next section.

3 Finite-Element Formulation of the Elbow Element

The analysis of a general assemblage of finite elements consists in essence of the formulation of the equilibrium equations of each individual element and the subsequent application of general solution procedures that are independent of the type of element considered [9]. Therefore, in the following discussion, we only need to focus our attention on the derivation of the equilibrium equations of a typical elbow element.

Using the principle of virtual work (or principle of minimum total potential energy) to derive the equilibrium equations that govern the linear response of a general finite element, we obtain [9]

$$\mathbf{K}\,\mathbf{U} = \mathbf{R} \tag{6}$$

where $\mathbf{K}$ is the stiffness matrix of the finite element corresponding to the element nodal point degrees-of-freedom listed in $\mathbf{U}$,

$$\mathbf{K} = \int_V \mathbf{B}^T\,\mathbf{C}\,\mathbf{B}\,dv \tag{7}$$

and $\mathbf{R}$ is the effective nodal point load vector [9]. In equation (7) $\mathbf{B}$ is the strain-displacement matrix, and $\mathbf{C}$ is the corresponding stress-strain matrix [9]. Considering the pipe elbow element we therefore only need to establish the $\mathbf{B}$ matrix and discuss how the integration in equation (7) is performed efficiently.

3.1 Evaluation of the Strain-Displacement Matrix. Using the concepts of finite-element analysis, we need to describe the geometry and variations of internal element displacements of a typical pipe element in terms of its nodal point quantities. Fig. 2 shows a generic pipe elbow element with the assumed four nodal points. To establish the geometry and displacement interpolation functions of the element, assume first that the pipe cross section does not ovalize. In this case the coordinate and displacement interpolations are as used in the isoparametric finite-element formulations of beam, plate, and shell elements discussed in [15, 17–20]. For completeness of the formulation of the elbow element we briefly summarize first the isoparametric beam element formulation that does not include ovalization.

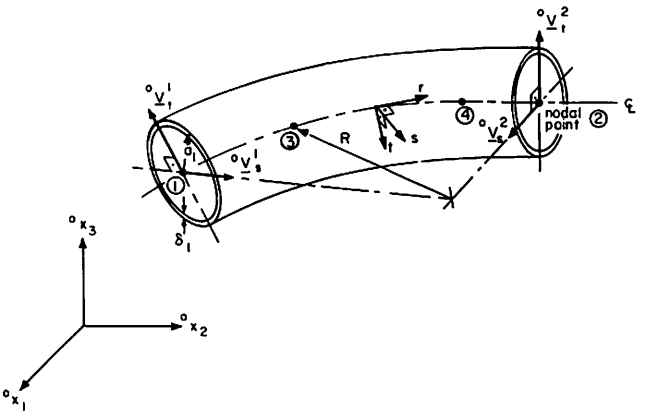

Fig. 2 Geometry of pipe elbow element

3.1.1 Element Geometry and Displacement Interpolations Assuming no Ovalization. The basic assumption in this formulation is that plane sections originally normal to the center-line axis of the pipe element remain plane but not necessarily normal to the center-line axis. Thus we can write the following equations for the coordinates of a point in the element before and after deformation:

$$^{l}x_i(r,s,t) = \sum_{k=1}^{4} h_k\,{}^{l}x_i^k + t\sum_{k=1}^{4} a_k h_k\,{}^{l}V_{ti}^k + s\sum_{k=1}^{4} a_k h_k\,{}^{l}V_{si}^k \qquad i = 1,2,3 \tag{8}$$

where

r, s, t = isoparameteric coordinates [9]
$^{l}x_i$ = Cartesian coordinate of any point in the pipe element
$h_k(r)$ = isoparametric interpolation functions
$^{l}x_i^k$ = Cartesian coordinate of nodal point k
a_k = outer radius of element at nodal point k
$^{l}V_{ti}^k$ = component i of unit vector $^{l}\mathbf{V}_t^k$, in direction t at nodal point k
$^{l}V_{si}^k$ = component i of unit vector $^{l}\mathbf{V}_s^k$, in direction s at nodal point k,

and the left superscript l denotes the configuration of the element; i.e., $l = 0$ denotes the original configuration, whereas $l = 1$ corresponds to the configuration in the deformed position.

The interpolation functions $h_k(r)$ used in equation (8) are derived in [9, pp. 127–130], and are summarized in Fig. 3. In the application of equation (8) it must be noted that the structural cross section considered is hollow, meaning that equation (8) is only applicable for the values of s and t that satisfy the equation

$$\left(1 - \frac{\delta_k}{a_k}\right)^2 \leq s^2 + t^2 \leq 1 \tag{9}$$

where δ_k and a_k are the wall thickness and the outside radius of the element at nodal point k. This fact is properly taken into account in the numerical integration to obtain the stiffness matrix of the element (see Section 3.3).

To obtain the displacement components at any point r, s, t in the pipe we have

$$u_i(r,s,t) = {}^{1}x_i - {}^{0}x_i \tag{10}$$

Thus, substituting from equation (8), we obtain

$$u_i(r,s,t) = \sum_{k=1}^{4} h_k u_i^k + t\sum_{k=1}^{4} a_k h_k V_{ti}^k + s\sum_{k=1}^{4} a_k h_k V_{si}^k \tag{11}$$

where

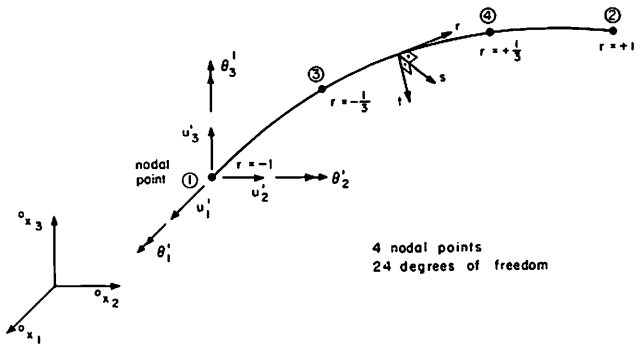

$$h_1 = [-9r^3+9r^2+r-1]/16$$
$$h_2 = [9r^3+9r^2-r-1]/16$$
$$h_3 = [27r^3-9r^2-27r+9]/16$$
$$h_4 = [-27r^3-9r^2+27r+9]/16$$

Fig. 3 Degrees-of-freedom and interpolation functions of pipe without ovalization

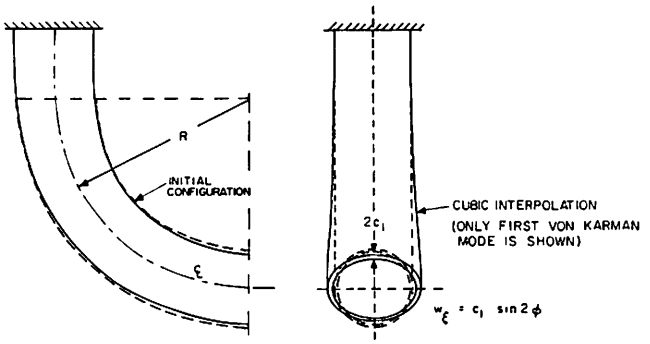

(a) ASSUMED VARIATION OF OVALIZATION ALONG ELBOW

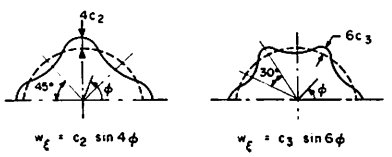

(b) SECOND AND THIRD VON KARMAN MODES

Fig. 4 Ovalization modes used in elbow formulation

$$V_{ti}^k = {}^1V_{ti}^k - {}^0V_{ti}^k$$
$$V_{si}^k = {}^1V_{si}^k - {}^0V_{si}^k \tag{12}$$

For the finite-element solution we express the components V_{ti}^k and V_{si}^k in terms of rotations about the global axes ${}^0x_i$, $i = 1, 2, 3$; namely, we have

$$\mathbf{V}_t^k = \boldsymbol{\theta}^k \times {}^0\mathbf{v}_t^k$$
$$\mathbf{V}_s^k = \boldsymbol{\theta}^k \times {}^0\mathbf{v}_s^k \tag{13}$$

where $\boldsymbol{\theta}^k$ is a vector listing the nodal point rotations at nodal point k, see Fig. 3,

$$\boldsymbol{\theta}^k = \begin{bmatrix} \theta_1^k \\ \theta_2^k \\ \theta_3^k \end{bmatrix} \tag{14}$$

Thus, substituting from equations (13) and (14) into equation (11), we obtain an equation that gives the displacement components $u_i(r, s, t)$ in terms of the nodal point displacements u_i^k and rotations θ_i^k, $i = 1, 2, 3$ and $k = 1, 2, 3, 4$.

3.1.2 Element Displacement Interpolations Including Ovalization. The displacement interpolations in equation (11) assume that the cross section of the pipe does not deform. To include the effect of ovalization we use the displacement patterns suggested by von Karman and others [2, 3, 5, and 6], and interpolate these displacement patterns cubically along the length of the elbow, see Fig. 4. Considering in-plane and out-of-plane action we use

$$w_\xi(r, \phi) = \underbrace{\sum_{m=1}^{N_c}\sum_{k=1}^{4} h_k c_m^k \sin 2m\phi}_{\text{in-plane bending}} + \underbrace{\sum_{m=1}^{N_d}\sum_{k=1}^{4} h_k d_m^k \cos 2m\phi}_{\text{out-of-plane bending}} \tag{15}$$

where the c_m^k and d_m^k, $k = 1, 2, 3, 4$, are the unknown generalized ovalization displacements. Depending on the pipe geometry, and the type of loading, it may be sufficient to include only the first, or first two, term(s) of one (or both) double summation(s) in equation (15), as discussed in Section 2.2 (see Table 1). In the implementation of the element we have allowed N_c to be 0 (no ovalization), 1, 2 or 3, and similarly for N_d.

The total pipe elbow displacements are the sum of the displacements given in equation (11) and equation (15). Thus a typical nodal point of a three-dimensional elbow element can have from 6 to 12 degrees of freedom at each node, depending on whether the ovalization displacements are included, and which ovalization patterns are used.

3.1.3 Displacement Derivatives. With the geometry and displacement interpolations given in equations (8), (11), and (15), in essence, standard procedures can be used to evaluate the appropriate displacement derivatives that constitute the elements of the strain-displacement matrix. Based on the discussion in Section 2.2 the complete strain-displacement relations for both in-plane and out-of-plane bending of the element can be written as

$$\begin{bmatrix} \epsilon_{\eta\eta} \\ \gamma_{\eta\xi} \\ \gamma_{\eta\zeta} \\ \epsilon_{\xi\xi} \end{bmatrix} = \sum_{k=1}^{4} \begin{bmatrix} \mathbf{B}^k & \mathbf{B}_{ov1}^k & \mathbf{B}_{ov3}^k \\ \mathbf{0} & \mathbf{B}_{ov2}^k & \mathbf{B}_{ov4}^k \end{bmatrix} \mathbf{u}^k \tag{16}$$

where

$$\mathbf{u}^{kT} = [u_1^k\, u_2^k\, u_3^k\, \theta_1^k\, \theta_2^k\, \theta_3^k \,|\, c_1^k\, c_2^k\, c_3^k \,|\, d_1^k\, d_2^k\, d_3^k] \tag{17}$$

In equation (16) all six ovalization patterns of equation (15) are included, but we could use less ovalization degrees of freedom.

The displacement derivatives in $\mathbf{B}^k$ correspond to the strains that are due to the beam bending nodal point displacements and rotations. Using equations (11)–(14) we have

$$\begin{bmatrix} u_{i,r} \\ u_{i,s} \\ u_{i,t} \end{bmatrix} = \sum_{k=1}^{4} \begin{bmatrix} h_{k,r}\,[1\ (g)_{1i}^k\ (g)_{2i}^k\ (g)_{3i}^k] \\ h_k\,[0\ (\hat{g})_{1i}^k\ (\hat{g})_{2i}^k\ (\hat{g})_{3i}^k] \\ h_k\,[0\ (\bar{g})_{1i}^k\ (\bar{g})_{2i}^k\ (\bar{g})_{3i}^k] \end{bmatrix} \begin{bmatrix} u_i^k \\ \theta_1^k \\ \theta_2^k \\ \theta_3^k \end{bmatrix} \tag{18}$$

where we employ the notation

$$(\hat{g})^k = a_k \begin{bmatrix} 0 & -{}^0V_{s3}^k & {}^0V_{s2}^k \\ {}^0V_{s3}^k & 0 & -{}^0V_{s1}^k \\ -{}^0V_{s2}^k & {}^0V_{s1}^k & 0 \end{bmatrix} \tag{19}$$

$$(\bar{g})^k = a_k \begin{bmatrix} 0 & -{}^0V_{t3}^k & {}^0V_{t2}^k \\ {}^0V_{t3}^k & 0 & -{}^0V_{t1}^k \\ -{}^0V_{t2}^k & {}^0V_{t1}^k & 0 \end{bmatrix} \tag{20}$$

and

$$(g)^k_{ij} = s(\hat{g})^k_{ij} + t(\bar{g})^k_{ij} \tag{21}$$

To obtain the displacement derivatives corresponding to the axes ${}^0x_i$, $i = 1, 2, 3$ we employ the Jacobian transformation

$$\frac{\partial}{\partial {}^0\mathbf{x}} = \mathbf{J}^{-1}\frac{\partial}{\partial \mathbf{r}} \tag{22}$$

where the Jacobian matrix, $\mathbf{J}$, contains the derivatives of the coordinates ${}^0x_i$, $i = 1, 2, 3$ with respect to the isoparametric coordinates r, s, and t [9]. Substituting from equation (18) into equation (22) we obtain

$$\begin{bmatrix} \frac{\partial u_i}{\partial {}^0x_1} \\ \frac{\partial u_i}{\partial {}^0x_2} \\ \frac{\partial u_i}{\partial {}^0x_3} \end{bmatrix} = \sum_{k=1}^{4} \begin{bmatrix} h_{k,1}(G1)^k_{i1}(G2)^k_{i1}(G3)^k_{i1} \\ h_{k,2}(G1)^k_{i2}(G2)^k_{i2}(G3)^k_{i2} \\ h_{k,3}(G1)^k_{i3}(G2)^k_{i3}(G3)^k_{i3} \end{bmatrix} \begin{bmatrix} u^k_i \\ \theta^k_1 \\ \theta^k_2 \\ \theta^k_3 \end{bmatrix} \tag{23}$$

where

$$(Gm)^k_{in} = (J^{-1}_{n1}(g)^k_{mi})h_{k,r} + (J^{-1}_{n2}(\hat{g})^k_{mi} + J^{-1}_{n3}(\bar{g})^k_{mi})h_k \tag{24}$$

Using the displacement derivatives in equation (23) we can now directly calculate the elements of the matrix $\mathbf{B}^k$; namely, equation (23) is used to establish the global strain components (corresponding to the ${}^0x_i$, $i = 1, 2, 3$, axes), and these components are transformed to the local strain components $\epsilon_{\eta\eta}$, $\gamma_{\eta\xi}$, and $\gamma_{\eta\zeta}$ to obtain the elements of the matrix $\mathbf{B}^k$.

The elements of the matrices $\mathbf{B}^k_{ov1}$, $\mathbf{B}^k_{ov2}$, $\mathbf{B}^k_{ov3}$, and $\mathbf{B}^k_{ov4}$ correspond to the entries labeled TERM 2 and TERM 3 in equation (4).

Thus, using equation (15) to interpolate w_ξ, we have

$$\mathbf{B}^k_{ov1} = \frac{h_k}{R - a\cos\phi}\begin{bmatrix} a_1 & a_2 & a_3 \\ 0 & 0 & 0 \\ 0 & 0 & 0 \end{bmatrix} \tag{25}$$

where

$$a_l = m\cos(m\phi)\cos\phi + \sin(m\phi)\sin\phi$$

ϕ = angular position in the cross section; see Fig. 1

$m = 2l$

and

$$\mathbf{B}^k_{ov2} = \frac{h_k}{a^2}[b_1\, b_2\, b_3] \tag{26}$$

where

$$b_l = -m(m^2 - 1)\cos(m\phi)\zeta \tag{27}$$

and

$$\mathbf{B}^k_{ov3} = \left(\frac{h_k}{R - a\cos\phi}\right)\begin{bmatrix} \tilde{a}_1 & \tilde{a}_2 & \tilde{a}_3 \\ 0 & 0 & 0 \\ 0 & 0 & 0 \end{bmatrix} \tag{28}$$

where

$$\tilde{a}_l = -m\sin(m\phi)\cos\phi + \cos(m\phi)\sin\phi, \tag{29}$$

and

$$\mathbf{B}^k_{ov4} = \frac{h_k}{a^2}[\delta_1\, \delta_2\, \delta_3] \tag{30}$$

where

$$\delta_l = m(m^2 - 1)\sin(m\phi)\zeta \tag{31}$$

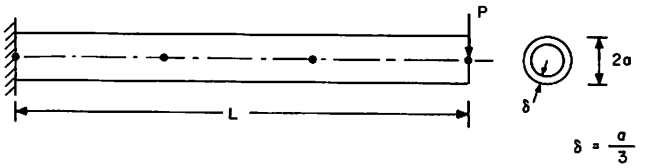

E = YOUNG'S MODULUS

I = MOMENT OF INERTIA

$\delta_{TH} = \frac{PL^3}{3EI}$

$\phi_{TH} = \frac{PL^2}{2EI}$

L/2a	$\frac{\delta - \delta_{TH}}{\delta_{TH}}$	$\frac{\phi - \phi_{TH}}{\phi_{TH}}$
10	.007042	.0000
100	.000071	.0000
1,000	.000001	.0000
10,000	.000000	.0000

Fig. 5 Analysis of cantilever straight pipe using a one element model

3.2 Stress-Strain Matrix. The stress-strain matrix used in the analysis corresponds to plane stress conditions in the $\xi - \eta$ plane, i.e., we use

$$\begin{bmatrix} \sigma_{\eta\eta} \\ \sigma_{\eta\xi} \\ \sigma_{\eta\zeta} \\ \sigma_{\xi\xi} \end{bmatrix} = \frac{E}{1-\nu^2}\begin{bmatrix} 1 & 0 & 0 & \nu \\ 0 & \frac{1-\nu}{2} & 0 & 0 \\ 0 & 0 & \frac{1-\nu}{2} & 0 \\ \nu & 0 & 0 & 1 \end{bmatrix}\begin{bmatrix} \epsilon_{\eta\eta} \\ \gamma_{\eta\xi} \\ \gamma_{\eta\zeta} \\ \epsilon_{\xi\xi} \end{bmatrix} \tag{32}$$

where E is the Young's modulus and ν the Poisson ratio of the material.

3.3 Numerical Integration. To evaluate the stiffness matrix in equation (7) we are using numerical integration. In linear analysis it may be possible and more effective to evaluate some of the integrations required in closed form, but in general nonlinear analysis numerical integration must be employed. Since our final objective is to use the element in nonlinear analysis, we choose to employ in all analyses numerical integration.

Much emphasis has been given in recent years to reduced numerical integration in the use of low-order beam and plate elements [17,21]. The use of reduced integration is necessary in those cases, because if the stiffness matrices of very thin low-order elements are evaluated accurately, the elements display much too stiff a behavior. Using reduced integration in the evaluation of the low-order element stiffness matrices can drastically improve some analysis results, but may also introduce spurious zero or very small eigenvalues that result in solution difficulties, and make it difficult to assess the reliability of the solution results in general (and particularly nonlinear) analysis. On the other hand, using the higher-order element presented in this paper reduced numerical integration is not needed for an accurate response prediction, and a reliable and effective solution is obtained using high-order integration (see also Section 4.1) [18,20].

Considering the assumed displacement distributions for the elbow element, the Newton-Cotes formulas can be employed for the numerical integration with the following integration orders: 3-point integration through the wall thickness, 5-point integration along the elbow, and, using the composite trapezoidal rule around the circumference, 12-point integration for in-plane loading, and 24-point integration for out-of-plane loading [9]. This integration order around the circumference assumes that all 3 ovalization patterns are included in the analysis; less integration stations can be employed if a smaller

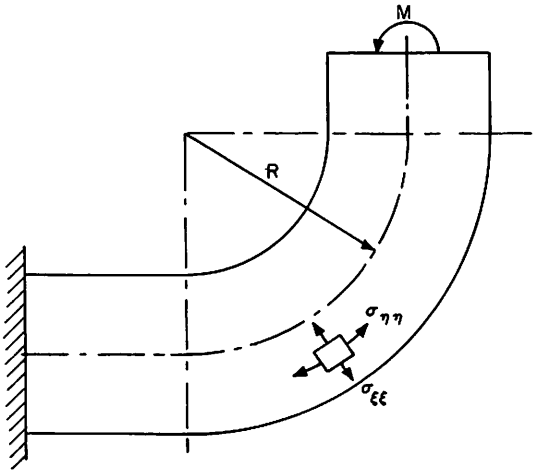

a) PIPE STRUCTURE; $R/a = 3.07$, $a/\delta = 20.8$, $\nu = .3$

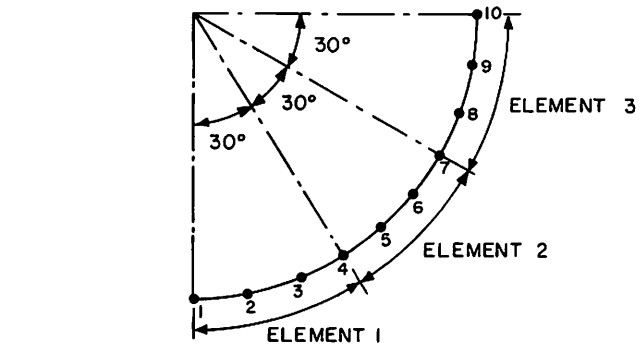

b) THREE ELEMENT MODEL (CENTRE LINE OF ELEMENTS AND NODAL POINTS ARE SHOWN)

Fig. 6 Pipe bend and finite-element model used

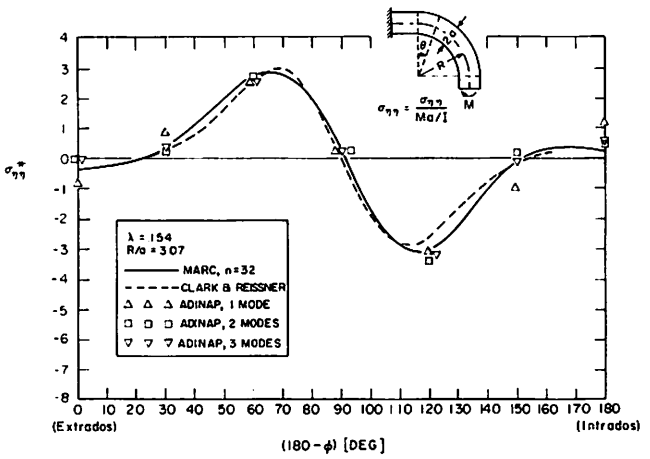

Fig. 7 Longitudinal stress at midsurface of bend in Fig. 6 (no end constraints)

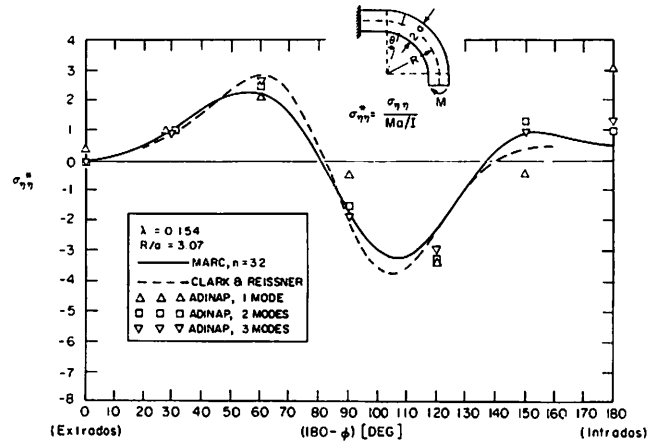

Fig. 8 Longitudinal stress at inside surface of bend in Fig. 6 (no end constraints)

number of ovalization degrees of freedom are used. Also, instead of the Newton-Cotes formulas, Gauss numerical integration could be employed. The choice of the integration scheme is particularly crucial in nonlinear analysis and we will be presenting more details on the numerical integration in future communications.

4 Sample Analyses

The elbow element has been implemented in the computer program ADINAP. The following analysis results are presented to indicate the applicability and effectiveness of the element. In all analyses the Newton-Cotes integration described in Section 3.3 was employed, and the pipe geometric factor used was $\lambda = R\delta/(a^2\sqrt{1-\nu^2})$ [12].

4.1 Analysis of a Straight Pipe. The straight cantilever pipe in Fig. 5 was analyzed to demonstrate the effectiveness of the element in the analysis of thin structural members. The element formulation includes shear deformations at a pipe cross section and it is instructive to evaluate this assumption in the solution of this problem. In the analysis one element was used to model the complete pipe.

Fig. 5 compares the analysis results obtained with the elementary beam theory solution for different length to diameter ratios. As expected, the displacements and stresses predicted using ADINAP are very close to those of elementary beam theory neglecting shear deformations for large length-to-diameter ratios, because in those cases the shear deformations contribute negligibly to the tip displacement of the pipe. Hence, it can be concluded that the element is effective when shear deformation effects can be neglected, which is the case in thin-walled pipes.

4.2 Analysis of a Pipe Bend. The pipe structure shown in Fig. 6 was analyzed using ADINAP because the analysis results could be compared with the results presented by Sobel [12]. Using ADINAP the pipe bend was modeled using three equal elbow elements as shown in Fig. 6.

In his work Sobel used the state-of-the-art tools provided in the MARC computer program to analyze the bend. Based on an extensive convergence study, Sobel concluded that 32 or 64 of the MARC pipe-bend segment elements need be used to model the bend.

In the first analysis using ADINAP the ovalization degrees of freedom at nodes 1 and 10 (and 2 to 9, see Fig. 6) were left free to simulate the conditions that were assumed in the analysis by Sobel. Figs. 7 to 9 show some stress components calculated using ADINAP and the corresponding results obtained by Sobel using the MARC program and the Clark and Reissner shell theory. The ADINAP analysis was performed using the 1, 2, and 3 in-plane bending ovalization terms of equation (15). Good correspondence between the ADINAP, MARC, and Clark and Reissner shell theory results is observed. It is also noted that in the ADINAP analysis all three terms of ovalization had to be included for an accurate response prediction, which corresponds to the recommendation given in Table 1. In the subsequent analysis of this bend we therefore included all the terms of ovalization.

In the second analysis using ADINAP the ovalization degrees of

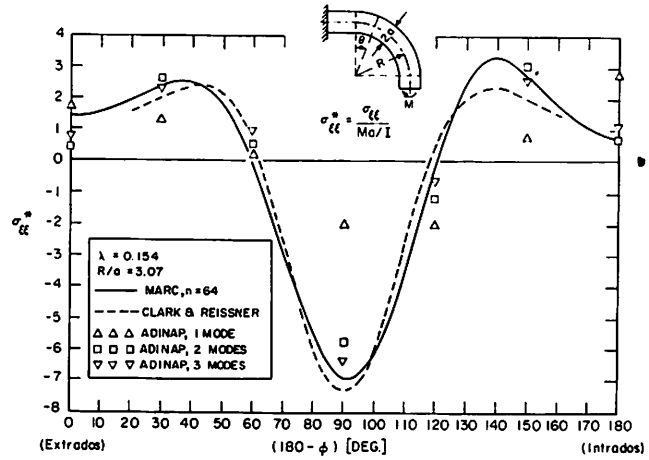

Fig. 9 Hoop stress at inside surface of bend in Fig. 6 (no end constraints)

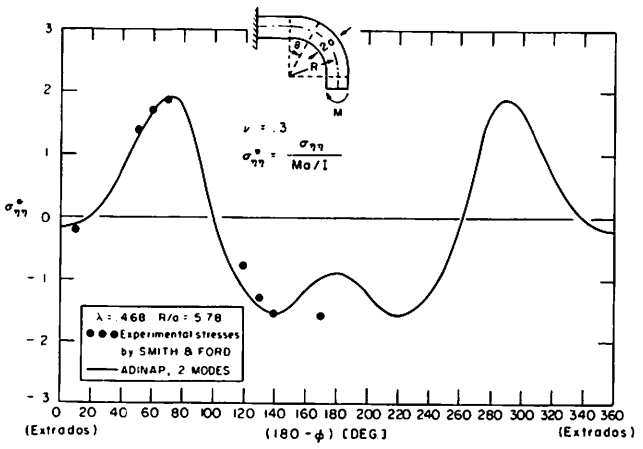

Fig. 12 Longitudinal stress at outside surface and at $\theta = 45°$ of Smith and Ford bend subjected to an in-plane bending moment

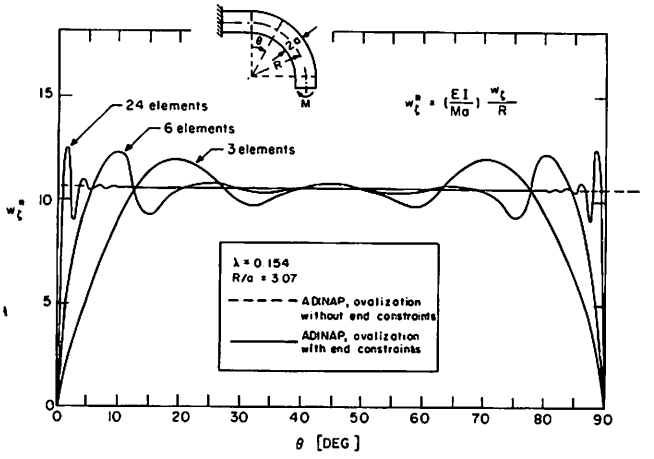

Fig. 10 Radial displacement w_ζ at $\phi = 90°$ of bend in Fig. 6 (3 ovalization modes)

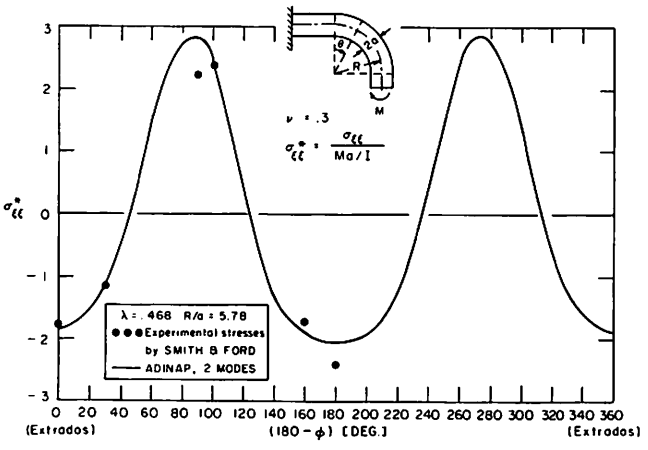

Fig. 13 Hoop stress at outside surface and at $\theta = 45°$ of Smith and Ford bend subjected to an in-plane bending moment

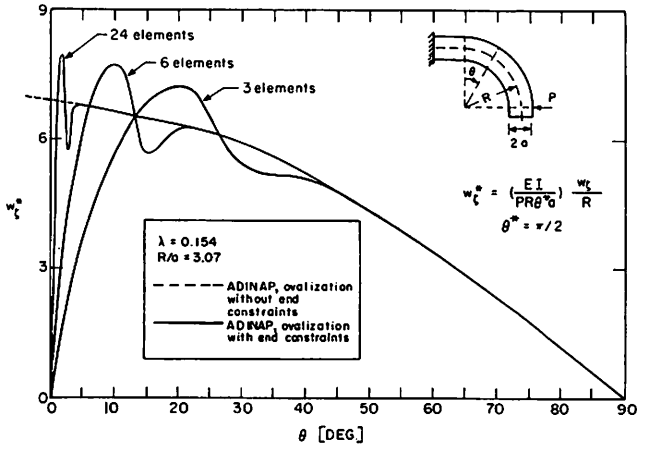

Fig. 11 Radial displacement w_ζ at $\phi = 90°$ of bend in Fig. 6 subjected to a concentrated force (3 ovalization modes)

freedom were set equal to zero at the two ends of the pipe. Fig. 10 shows the variation of ovalization along the pipe bend predicted in this analysis, using 3, 6, and 24 equal elements to model the bend. As expected the finite-element results converge (neglecting the initial overshoot/undershoot) to the analytical solution that is based on the von Karman theory. It should be noted that this theory does not account for elbow end-effects and using this theory there is a stress singularity at $\theta = 0°$ and 90°; therefore, the present elbow element cannot be used to predict the stresses accurately at the elbow ends.

In the third analysis, the pipe structure was subjected to a concentrated transverse load instead of the concentrated moment. Fig. 11 shows the predicted ovalization again using 3, 6 and 24 equal elements to model the bend. It is seen that the finite-element results converge (again neglecting the initial overshoot/undershoot) to the ovalization predicted by the von Karman theory.

4.3 In-Plane and Out-of-Plane Bending Analysis of a Second Pipe Bend. The second pipe bend shown in Figs. 12–15 was analyzed for in-plane and out-of-plane bending using the same finite-element mesh as was employed in the previous analysis (see Fig. 6(*b*)). Some longitudinal and hoop stress results calculated with ADINAP are shown for the in-plane bending in Figs. 12 and 13, and for the out-of-plane bending in Figs. 14 and 15. The computed results are compared in the figures with experimentally obtained values [22] and good correspondence is noted.

5 Conclusions

The formulation of a simple and versatile pipe elbow element has been presented. The element has been implemented and the solution results of various sample analyses have been presented. Since the element has been formulated using basically beam theory plus an allowance for ovalization of the elbow cross section, the element cannot capture the full three-dimensional shell behavior of elbows,

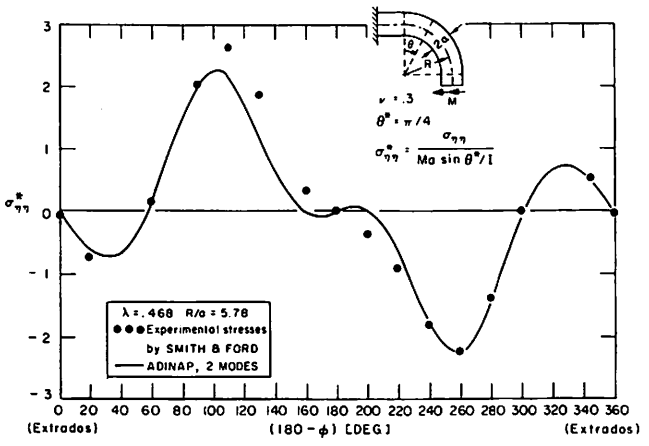

Fig. 14 Longitudinal stress at outside surface and at $\theta = 45°$ of Smith and Ford bend subjected to an out-of-plane bending moment

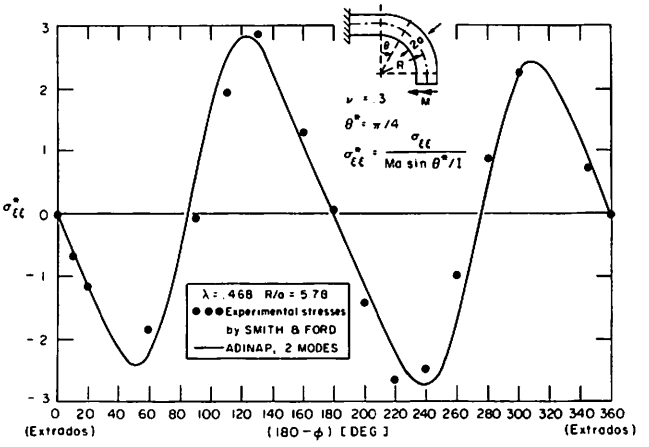

Fig. 15 Hoop stress at outside surface and at $\theta = 45°$ of Smith and Ford bend subjected to an out-of-plane bending moment

if activated. However, the element predicts the significant displacements and stresses accurately for a large range of pipe geometries, and for the same accuracy, the use of the element leads to very much less expensive solutions than other previously published computational tools.

The approach employed in the formulation of the elbow element shows much promise for the development of a simple and effective element that can also model accurately elbow end-effects, internal pressure effects and, in particular, nonlinear material and geometric behavior.

Acknowledgment

We gratefully acknowledge the financial support of A. D. Little, Cambridge, Mass., for the development of the elbow element, and the support of CNEN, Brazil, for C. Almeida's studies.

References

1 Rodabaugh, E. C., and Pickett, A. G., "Survey Report on Structural Design of Piping Systems and Components," EID-25553, Dec. 1970.

2 Vigness, I. "Elastic Properties of Curved Tubes," TRANS. ASME, Vol. 55, 1943, pp. 105–120.

3 Pardue, T. W., and Vigness, I., "Properties of Thin-Walled Curved Tubes of Short-Bend Radius," TRANS. ASME, Vol. 73, 1951, pp. 74–84.

4 Gross, N., and Ford, H., "The Flexibility of Short-Radius Pipe Bends," *Proceedings of the Institution of Mechanical Engineers*, 1952–1953, pp. 480–491.

5 Dodge, W. G., and Moore, S. E., "Stress Indices and Flexibility Factors for Moment Loadings on Elbows and Curved Pipes," *Welding Research Council Bulletin 179*, Dec. 1972.

6 von Karman, T., "Über die Formänderung Dünnwanndiger Rohre, Innsbesondere Federnder Ausgleichrohre," *Zeitschrift des Vereines deutscher Ingenieure*, Vol. 55, 1911, pp. 1889–1895.

7 Turner, C. E., and Ford, H., "Examination of the Theories for Calculating the Stresses in Pipe Bends Subject to In-Plane Bending," *Proceedings of the Institution of Mechanical Engineers*, Vol. 171, 1957, pp. 513–525.

8 Clark, R. A., and Reissner, E., "Bending of Curved Tubes," *Advances in Applied Mechanics*, Vol. 2, 1951, pp. 93–122.

9 Bathe, K. J., and Wilson, E. L., *Numerical Methods in Finite Element Analysis*, Prentice-Hall, Englewood Cliffs, N.J., 1976.

10 MARC—CDC, Nonlinear Finite Element Analysis Program, MARC Analysis Corporation, Palo Alto, Calif., and Control Data Corporation, Minneapolis, Minn., 1974.

11 Shimizu, T., et al., "Some Experiences on Elastic-Plastic Analysis of Shell Structures," *Applications Using ADINA, Proceedings of the ADINA Conference*, Aug. 1977, Bathe, K. J., ed., Report AVL 82448-6, Department of Mechanical Engineering, M.I.T., Aug 1977.

12 Sobel, L. H., "In-Plane Bending of Elbows," *Journal of Computers and Structures*, Vol. 7, 1977, pp. 701–715.

13 Ohtsubo, H., and Watanabe, O., "Stress Analysis of Pipe Bends by Ring Elements," TRANS. ASME, Vol. 100, Feb. 1978, pp. 112–122.

14 Bathe, K. J., Ramm, E., and Wilson, E. L., "Finite Element Formulations for Large Deformation Dynamic Analysis," *International Journal for Numerical Methods in Engineering*, Vol. 9, 1975, pp. 353–386.

15 Bathe, K. J., "Finite Element Formulation, Modeling, and Solution of Nonlinear Dynamic Response," Chapter in *Numerical Methods for Partial Differential Equations*, Parter, S. V., ed., Academic Press, 1979.

16 NONPIPE—ADINAP, Reference [1], Arthur D. Little Report 1979.

17 Zienkiewicz, O. C., *The Finite Element Method*, McGraw-Hill, New York, 1977.

18 Ramm, E., "A Plate/Shell Element for Large Deflections and Rotations," in *Formulations and Computational Algorithms in Finite Element Analysis*, Bathe, K. J., Oden, J. T., and Wunderlich, W., eds., M.I.T. Press, 1977.

19 Kråkeland, B., and Mo, O., "Nonlinear Analysis of Stiffened Shells," *Proceedings of the 7th Structural Analysis S.I.G. Meeting*, Sperry Univac, Nice, France, Oct. 1978.

20 Bathe, K. J., and Bolourchi, S., "A Geometric and Material Nonlinear Plate and Shell Element," *Journal Computers and Structures*, in press.

21 Hughes, T. J. R., Taylor, R. L., and Kanoknukulchai, W., "A Simple and Efficient Finite Element for Plate Bending," *International Journal for Numerical Methods in Engineering*, Vol. 11, 1977, pp. 1529–1543.

22 Smith, R. T., and Ford, H., "Experiments on Pipelines and Pipe Bends Subjected to Three-Dimensional Loading," *Journal of the Mechanical Engineering Sciences*, Vol. 9, 1967, pp. 124–135.